Experimental Characterisation of Tilt Stabilisation within Passively Levitated Electrodynamic Thrust Self-Bearing Motors

1st Joachim Van Verdeghem, *Student Member, IEEE*, 2nd Bruno Dehez, *Senior Member, IEEE*
Mechatronic, Electrical Energy, and Dynamic systems (MEED), Institute of Mechanics,
Materials and Civil Engineering (IMMC), Université catholique de Louvain (UCLouvain)
Louvain-la-Neuve, Belgium
joachim.vanverdeghem@uclouvain.be

***Abstract*—*Abstract* — Despite the significant advantages regarding their reliability and compactness, the interest in passively levitated self-bearing (bearingless) machines is fairly new due to the difficulty to circumvent limitations underlined by Earnshaw's theorem. Nevertheless, electrodynamic thrust bearings (EDTBs) have proved, first at the modelling and then at the experimental level, their ability to combine, within one single multifunction winding, the rotor passive axial levitation and the drive function, leading to electrodynamic thrust self-bearing (EDTSB) machines. Besides, an electromechanical model highlighted that, considering a specific connection of the armature winding, these bearings can also generate an electrodynamic torque counteracting the rotor tilt. This paper takes a step further by transposing and validating this principle and the underlying model to EDTSB machines. Consequently, self-bearing machines achieving fully passive magnetic levitation could be designed by the addition of one single permanent magnet centring bearing.**

Index Terms*—*Topic* — *High speed motors, bearingless motors and magnetic bearings

I. Introduction

Bearingless or self-bearing motors (SBMs) provide, within one single unit, both the conventional drive function and the rotor guidance. Their development has been supported by the increasing demand for machines operating in high purity environment, requiring a high compactness or rotating at high spin speeds. Traditionally, they comprise two separate windings, each of them being devoted either to the torque production or to the rotor magnetic levitation. However, aiming at increasing their power density as well as reducing the Joules losses and the mechanical complexity of the system, much research efforts have been concentrated on the combination of these two functions within one single multifunction winding [1]–[3].

Nowadays, to the authors' best knowledge, in all self-bearing machines, the rotor suspension lean on the active control of the current flowing in the armature winding for at least one degree of freedom, implying that dedicated sensors, controllers and power electronics are required. Discarding these elements would allow to increase the compactness and reliability of the system. Despite these attractive benefits, very little attention has so far been paid to the design of SBMs whose rotor guidance solely relies on passive phenomena. More precisely, recent researches have disclosed that centring electrodynamic bearings (EDBs) can produce, in addition to the classic passive restoring force, a drive torque thanks to a smart connection of the power supply to the armature winding [4]. The performance of this particular machine have been investigated experimentally under quasi-static conditions, i.e. static rotor eccentricity and constant spin speed, validating in particular the working principle [5]. Nevertheless, the radial motion of these SBMs suffers from critical dynamic instability issues typical of EDBs, thus requiring the addition of external non-rotating damping.

In contrast, electrodynamic thrust bearing (EDTBs) are stable in the usual spin speed range and have thus been the starting point for the design of new SBMs [6]. Among them, an EDTB including additional coils to drive the rotor has been studied experimentally [7]. Later on, the significant number of similarities between these bearings and axial flux PM machines has led to the development of a passively levitated electrodynamic thrust self-bearing (EDTSB) motor, combining, within one multifunction winding, both the rotor axial suspension and the drive function. In addition, an electromechanical model allowing us to describe its axial and spin dynamics has been derived [8]. This machine was successfully implemented and tested in a dedicated setup, underlining its ability to passively levitate the axial degree of freedom of the rotor. Furthermore, the dynamical model has been corroborated through measurements, validating the independence of the axial dynamics to the motor currents [9].

Considering a specific connection of the armature winding, EDTBs can exert, in addition to the classic axial restoring force, an electrodynamic torque counteracting the rotor tilt, implying that both tilt degrees of freedom could also be stabilised through passive phenomena [10]. Hence, the radial guidance could be provided by one single permanent magnet centring bearing, thus increasing the system compactness. Under the assumption of small rotor displacements, an electromechanical model allowing us to study the five degrees of freedom of these bearings has been developed, highlighting that the axial and

J. Van Verdeghem is a FRIA Grant Holder of the Fonds de la Recherche Scientifique-FNRS, Belgium.

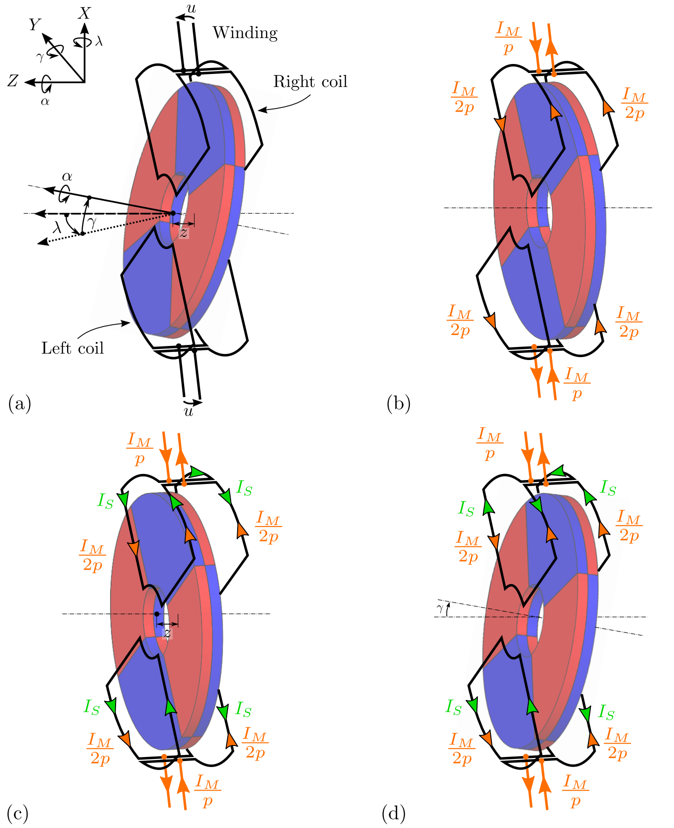

Fig. 1: Schematic representations of EDTSB motor topologies with $p = 2$ and limited to one phase. (a) Topology. (b) Centred position. (c) Axial displacement ($z \neq 0$). (d) Tilt ($\gamma \neq 0$).

tilt dynamics are decoupled and that no electrodynamic effects ensue from a rotor radial eccentricity [11]. Nevertheless, to date, experimental results still lack to endorse this principle as well as the corresponding dynamical model. In addition, applying this particular winding connection to EDTSB machines should allow to gather, within this multifunction winding, both the passive tilt and axial magnetic suspensions to the drive function. Consequently, combining this machine with one single PM centring bearing would lead to a compact and reliable fully passive magnetic suspension.

In this context, this paper is devoted to the experimental validation of the tilt stabilisation within passively levitated electrodynamic thrust self-bearing machines through the analysis of the armature winding flux linkage and the electrodynamic torque ensuing from a tilt deflection.

The paper is structured as follows. Section II describes the structure of EDTSB machines as well as their operation principle. Following on from this, section III presents the electromechanical model allowing us to study the tilt stabilisation. Finally, section IV and V are respectively dedicated to the description of the prototype and its test rig and to the experimental characterisation performed on their basis.

II. Operation Principle

A. Structure

As represented in Fig. 1(a), the self-bearing motor considered in this study has an identical structure to classic axial flux double-sided double-stator single-rotor permanent magnet (PM) machines. More precisely, the rotor comprises an arrangement of axially magnetised PM with alternate polarisation generating an axial magnetic field having p pole pairs. Regarding the stator, the armature winding encompasses N phases, each of them consisting in p identical and evenly distributed windings. The latter are themselves formed by the parallel connection of a left and a right coil and are all connected in parallel to the power supply. Let us point out the winding configuration has a significant impact on the machine behaviour given that, rather considering a series connection of the p left and the p right coils independently, both resulting windings being connected in parallel to the voltage source, no electrodynamic effect and therefore restoring torque would ensue from the rotor tilt [11].

B. Centred position

As represented in Fig. 1(b), in the nominal position, the fluxes linked by the left and right coils of each winding are identical. The resulting electromotive forces are therefore equal and the motor current I_M, provided by the power supply u, follows a balanced distribution between the $2p$ coils. As stated by Laplace law, by their interaction with the PM magnetic field, these currents generate, as in classic PM machines, a drive torque whereas neither an axial force nor a tilt torque are produced.

C. Axial displacement

Considering a rotor axial deviation from its equilibrium position, namely $z \neq 0$, the flux linkages and therefore the electromotive forces induced in the left and right coils of each winding are no more identical, thus leading to an unbalanced distribution of the motor current between these two coils. In fact, assuming small axial rotor displacements, these flux linkages vary linearly with the axial position z, implying that, in comparison with the equilibrium position, one coil undergoes an increase I_S of its current while the other one a reduction by the same quantity, as illustrated in Fig. 1(c). Consequently, for each winding, the left and right currents can be seen as the superposition of the classic motor current, flowing in both coils connected in parallel, with a suspension current I_S circulating in a short-circuited path formed by the series connection of these two coils. The former current produces a drive torque unchanged with respect to the centred position whereas the latter generates an axial force that restores the rotor in its nominal position as well as a drag torque.

D. Tilt

Considering now a rotor tilt, i.e. $(\lambda\,;\gamma) \neq (0\,;0)$, as shown in Fig. 1(d), the fluxes linked by the left and right coils of each winding are not equal either. However, in contrast with an axial rotor off-centring, the p left as well as the p right flux linkages also differ. Consequently, still assuming small rotor displacements, the currents flowing in the left and right coils can be seen as the superposition of the classic motor current, leading to the production of the drive torque, with a suspension current I_S that may be different in each winding and results in an electrodynamic torque parallel to the tilt recentring the rotor, a torque perpendicular to the tilt engendering a parasitic precession motion as well as a drag torque counteracting the classic motor torque.

III. Electromechanical Model

Under the assumption of small axial, radial and tilt deflections, the fluxes $\phi_{k,L}$ and $\phi_{k,R}$ respectively linked by the k-th left and right coils can be expressed as [11]:

$$\begin{aligned} \phi_{k,l} &= (\Phi_0 \pm zK_z)\cos(p(\delta_k - \alpha)) \\ &\mp K_{\beta,p+1}[\gamma\cos((p+1)\delta_k - p\alpha) - \lambda\sin((p+1)\delta_k - p\alpha)] \\ &\mp K_{\beta,p-1}[\gamma\cos((p-1)\delta_k - p\alpha) + \lambda\sin((p-1)\delta_k - p\alpha)], \end{aligned} \tag{1}$$

where $k = \{1, \ldots, Np\}$, the upper and lower signs correspond respectively to $l = L$ and $l = R$, $\delta_k = \frac{2\pi(k-1)}{pN}$ is the position of the k-th winding with respect to the X-axis, α is the rotor spin position, Φ_0 is the flux constant, K_z is the axial flux gradient, $K_{\beta,p+1}$ and $K_{\beta,p-1}$ are the tilt flux gradients respectively linked to the $p+1$ and $p-1$-th harmonics. These flux linkages present a linear dependence to the tilt deflections and differ in the p left as well as in the p right coils of each phase. Following an approach identical to that adopted in [8], it can be easily proved that the equations related to the axial and tilt levitation are independent from the motor currents and correspond to those describing electrodynamic thrust bearings. The latter have already been studied in detail, notably highlighting the decoupling that exists between these two dynamics [11]. Furthermore, as will be explained hereinafter, the present experimental validation relies on a test facility solely enabling, in addition to the rotor axial and spin motions, a one-degree-of-freedom tilt movement of the stator characterised by the angle γ. In these conditions, the tilt dynamic behaviour of the machine under study is governed by the following equations:

$$\begin{bmatrix} \ddot{\gamma} \\ \dot{\gamma} \\ \dot{T}_{\gamma,p-1} \\ \dot{T}_{\gamma,p+1} \\ \dot{T}_{\lambda,p-1} \\ \dot{T}_{\lambda,p+1} \end{bmatrix} = \mathbf{A} \begin{bmatrix} \dot{\gamma} \\ \gamma \\ T_{\gamma,p-1} \\ T_{\gamma,p+1} \\ T_{\lambda,p-1} \\ T_{\lambda,p+1} \end{bmatrix} + \begin{bmatrix} \frac{T_{\gamma,e}}{J_t} \\ 0 \\ 0 \\ 0 \\ 0 \\ 0 \end{bmatrix}, \tag{2}$$

$$\mathbf{A} = \begin{bmatrix} 0 & 0 & \frac{1}{J_t} & \frac{1}{J_t} & 0 & 0 \\ 1 & 0 & 0 & 0 & 0 & 0 \\ -\frac{2K^2_{\beta,p-1}Np}{L_{c,p-1}} & 0 & \frac{-2R}{L_{c,p-1}} & 0 & p\omega & 0 \\ -\frac{2K^2_{\beta,p+1}Np}{L_{c,p+1}} & 0 & 0 & \frac{-2R}{L_{c,p+1}} & 0 & -p\omega \\ 0 & -p\omega\frac{2K^2_{\beta,p-1}Np}{L_{c,p-1}} & -p\omega & 0 & \frac{-2R}{L_{c,p-1}} & 0 \\ 0 & p\omega\frac{2K^2_{\beta,p+1}Np}{L_{c,p+1}} & 0 & p\omega & 0 & \frac{-2R}{L_{c,p+1}} \end{bmatrix},$$

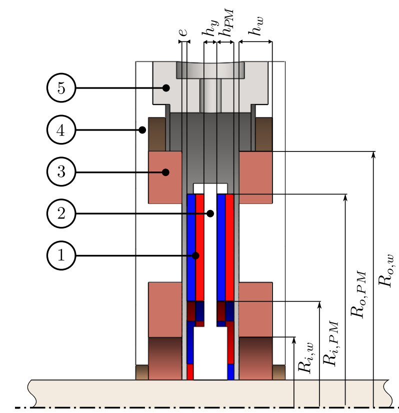

Fig. 2: Cross-sectional view of the prototype. 1 PM arrangement. 2 Ferromagnetic yoke. 3 Armature winding. 4 Non-magnetic non-conductive yoke. 5 Stator case.

TABLE I: Prototype dimensions (mm)

$R_{i,PM}$	$R_{o,PM}$	$R_{i,w}$	$R_{o,w}$	e	h_y	h_{PM}	h_w
25	50	20	55	1	3	4	5.1

where J_t is the transverse polar moment of inertia, R is the coil resistance, $L_{c,p+1}$ and $L_{c,p-1}$ are cyclic inductances, $T_{\gamma,e}$ is the tilt external torque, $T_{\gamma,p-1}$ and $T_{\gamma,p+1}$ are the torques parallel to the rotor tilt respectively related to the $p-1$ and $p+1$-th harmonics whereas $T_{\lambda,p-1}$ and $T_{\lambda,p+1}$ are their perpendicular parasitic counterparts inducing a precession motion.

Assuming quasi-static conditions, i.e. $\dot{z} = \dot{\gamma} = 0$ and a constant spin speed ω, the total torque T_γ ensuing from a tilt deflection γ can be retrieved from this model, yielding:

$$\begin{aligned} T_\gamma(\gamma,\omega) &= T_{\gamma,p-1} + T_{\gamma,p+1} \\ &= -\gamma\left(\frac{2K^2_{\beta,p-1}Np}{L_{c,p-1}}\frac{(p\omega L_{c,p-1})^2}{(p\omega L_{c,p-1})^2 + (2R)^2}\right. \\ &\qquad \left. + \frac{2K^2_{\beta,p+1}Np}{L_{c,p+1}}\frac{(p\omega L_{c,p+1})^2}{(p\omega L_{c,p+1})^2 + (2R)^2}\right). \end{aligned} \tag{3}$$

IV. Experimental Setup

The experimental setup described in this section aims at validating the working principle as well as the electromechanical model describing the axial and tilt stabilisation provided by electrodynamic thrust self-bearing machines.

A. Prototype

As illustrated in Fig. 2, the rotor includes two PM arrangements 1 placed in an attractive mode on both sides of a ferromagnetic yoke 2 and produces a six pole pair magnetic field ($p = 6$). The stator encompasses three phases ($N = 3$) consisting each in six left and six right full-pitched distributed coils 3. They comprise fifteen loops and are wound from 0.9 (mm) diameter Litz wire, to avoid parasitic eddy currents, on 3D printed non-magnetic non-conductive yokes 4, themselves being fixed on the stator case 5. The main dimensions are listed in Table I.

B. Test rig

Fig. 3(a) depicts the test rig designed to investigate the prototype axial, tilt and spin performances. As stated in section III, only one of the two tilt degrees of freedom is considered in this experimental characterisation, and, without having any impact on the machine operation, it is the stator that can tilt with respect to the frame and thus the rotor whereas the latter can solely move axially as well as rotate about its spin axis. This particular mounting facilitates the position and force measurements while reducing the test bench complexity.

Fig. 3(b) illustrates a cross-sectional view of the complete system taken along the plane $\boxed{\text{A}}$ that includes the EDTSB machine spin axis. The rotor radial and tilt degrees of freedom are guided through two air bearings (2) located on both sides of the prototype (1), therefore not affecting its axial dynamics. A capacitive displacement sensor (3) allows us to measure the rotor axial position. The conventional hall sensors and the encoder are replaced by one single contactless magnetic rotary sensor (4) providing, to a classic BLDC driver, the measurements necessary to control the rotor spin speed and position. An eddy current damper (5), consisting in up to four axially magnetised annular PMs separated by ferromagnetic parts and attached to the stator as well as a conductive sleeve surrounding the rotor, can be added to the system so as to increase the axial damping. A DC motor (6) can be fixed to the shaft right end pursuing two objectives. On the one hand, it can be employed to drive the rotor either to analyse the electromotive force induced in each coil or to study the axial and tilt bearing functions, remembering that the prototype is reduced to a classic EDTB in the absence of power supply. On the other hand, this motor can be considered as a load for the self-bearing machine under study. In both cases, the DC motor is guided with an air bearing (7) so as to allow us to measure the reaction axial force and spin torque through a six-axis force sensor (8). Lastly, the frame (9) can be tilted by an angle σ, measured from the horizontal by an inclinometer (10), with respect to the support (11). In this way, an external axial force $F_{z,e} = mg\sin\sigma$ can be exerted on the rotor, m being the rotor mass and g the acceleration due to gravity.

Fig. 3(c) represents a cross-sectional view of the test rig taken along plane $\boxed{\text{B}}$. The stator case (12) is supported by two air bearings (13) that ensure both its axial and radial guidances, thus leaving the armature winding a one-degree-of-freedom movement characterised by the angle γ, as mentioned above. Let us point out that the stator case (12) can also be shifted by 90 degrees so as to study the electromotive forces related to a rotor tilt λ. An inductive encoder (14) provides a high precision measurement of the stator tilt angle γ without affecting the underlying motion. It is worth noting that, the axial and tilt levitation leaning on passive electrodynamic phenomena, this sensor is employed for characterisation purposes only. Furthermore, an external torque $T_{\gamma,e}$ can be applied by suspending a mass to a pulley (15). Finally, a reaction torque sensor (16) can also be coupled to the stator in order to measure the restoring torque T_γ generated by the EDTSB machine.

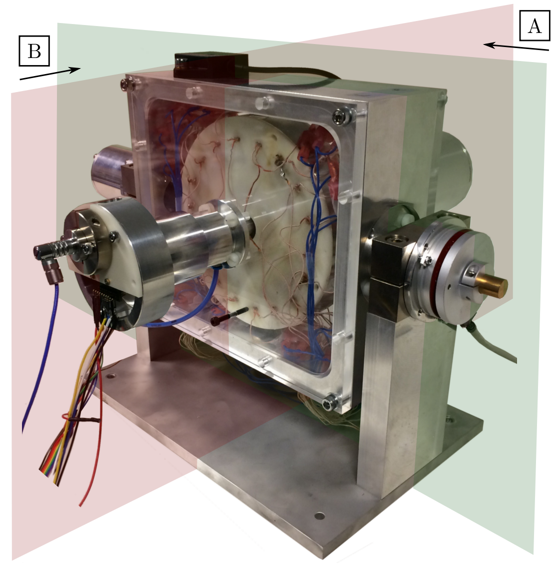

(a)

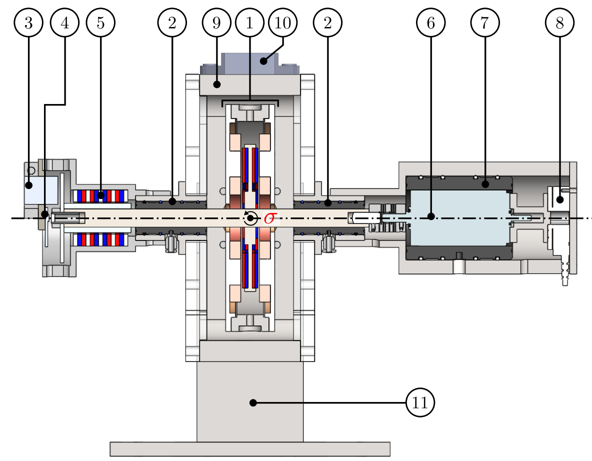

(b)

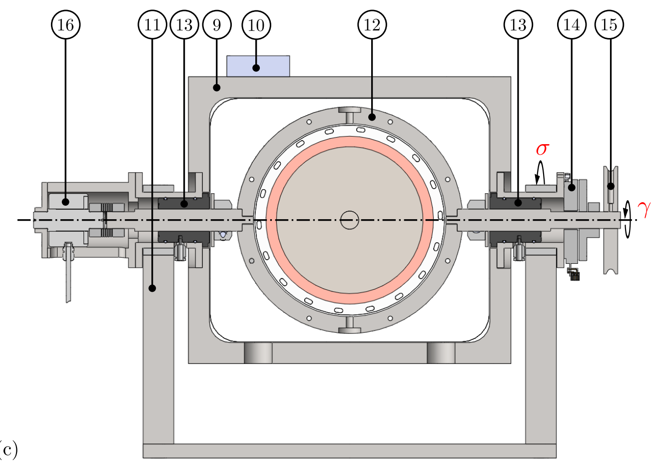

(c)

Fig. 3: Test rig: picture and cross-sectional views. (1) Prototype. (2) Air bearing. (3) Axial displacement sensor. (4) Spin position sensor. (5) Axial damper. (6) DC motor. (7) Air bearing. (8) Six-axis force sensor. (9) Frame. (10) Inclinometer. (11) Support. (12) Stator case. (13) Air bearing. (14) Tilt position sensor. (15) Pulley. (16) Torque sensor.

V. Experimental Characterisation

This section is devoted to the experimental investigation of the prototype described above through the analysis of the coil impedances, the flux linkages as well as the tilt stabilisation.

A. Coils Impedances

The electrodynamic phenomena, and therefore the underlying restoring forces, being highly dependent on the inductive or resistive behaviour of the armature, the winding impedances have to be determined. To this end, the resistance and inductance of each coil are measured through a RLC meter, leading respectively to 141 (mΩ) and 11.5 (μH) on average. In addition, the mutual inductance coefficients between them are identified, allowing us to calculate the three cyclic inductances upon which the axial and tilt stabilisations depend:

$$\begin{aligned} L_{c,p} &= 2\sum_{k=1}^{Np} L_{1k}\cos(p\delta_k) = 21.26\ (\mu\text{H}), \\ L_{c,p-1} &= 2\sum_{k=1}^{Np} L_{1k}\cos((p-1)\delta_k) = 25.75\ (\mu\text{H}), \\ L_{c,p+1} &= 2\sum_{k=1}^{Np} L_{1k}\cos((p+1)\delta_k) = 16.80\ (\mu\text{H}). \end{aligned} \tag{4}$$

B. Flux Linkages

The flux linked by the armature winding due to the PMs and, more specifically, its dependence to the rotor position lies at the basis of the axial and tilt levitation achieved within the self-bearing machine considered here. These flux linkages can be easily studied through the analysis of the electromotive force induced in each coil. Indeed, assuming quasi-static conditions, i.e. $\dot{z} = \dot{\lambda} = \dot{\gamma} = 0$ and a constant spin speed ω, the voltages $e_{k,L}$ and $e_{k,R}$ induced respectively in the k-th left and right coils can be expressed as follows:

$$\begin{aligned} e_{k,l} = -p\omega\big[&(\Phi_0 \pm zK_z)\sin(p(\delta_k-\alpha)) \\ &\mp K_{\beta,p+1}[\gamma\sin((p+1)\delta_k - p\alpha) + \lambda\cos((p+1)\delta_k - p\alpha)] \\ &\mp K_{\beta,p-1}[\gamma\sin((p-1)\delta_k - p\alpha) - \lambda\cos((p-1)\delta_k - p\alpha)]\big], \end{aligned} \tag{5}$$

where the upper and lower signs correspond respectively to $l = L$ and $l = R$. By convenience, let us focus on the impact of an axial displacement z and a tilt deflection γ on the left and right electromotive forces of the windings A_1 ($k = 1$) and A_4 ($k = 10$), the latter being reduced to:

$$\begin{aligned} e_{A1,l} &= p\omega[\Phi_0 \pm zK_z \mp \gamma(K_{\beta,p+1} + K_{\beta,p-1})]\sin(p\alpha), \\ e_{A4,l} &= p\omega[\Phi_0 \pm zK_z \pm \gamma(K_{\beta,p+1} + K_{\beta,p-1})]\sin(p\alpha). \end{aligned} \tag{6}$$

Indeed, as shown in Fig. 4, these windings are diametrically opposed and aligned with the X-axis, respectively implying that the deviations in the induced voltage ensuing from a tilt deflection γ are opposed and in phase with the electromotive force linked to the equilibrium position. Fig. 5 represents the time evolution of the voltage induced in the left and right coils of the windings A_1 and A_4 for three different relative positions between the rotor and the stator. As shown in Fig. 5(a), when

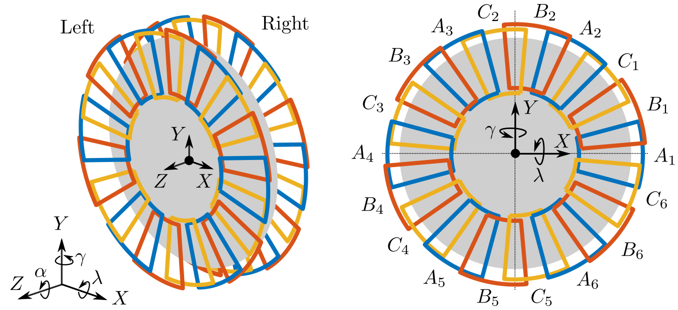

Fig. 4: Winding mechanical position.

the system is centred, i.e. $z = \gamma = 0$, these four induced voltages are identical and no suspension current thus circulates in the windings. By contrast, as illustrated in Fig. 5(b), when the rotor undergoes an axial displacement z, the electromotive forces related to the left coils are identical as well as those related to the right coils but both sides differ from each other. Similarly, considering now a tilt deflection γ, the voltages induced in both coils linked by a central symmetry, i.e. $A_{1,R}$ and $A_{4,L}$ as well as $A_{1,L}$ and $A_{4,R}$, follow an identical trend, as illustrated in Fig. 5(c). In both last cases, an unbalance between the left and right electromotive forces of each winding appears, leading to the circulation of suspension currents $I_{S,k}$ and therefore to the production of restoring forces.

Figs. 6(a) and 6(b) depict the evolution with the rotor axial position z and the tilt deflection γ of the amplitude of the fundamental of the flux linked by the left and right coils of the windings A_1 and A_4 respectively, the dots corresponding to the experimental data and the planes to linear regressions. The consistency between them, corroborated through coefficients of determination larger than 0.998, allows us to validate the linearisation of the flux linkages resulting from the assumption of small displacements. Furthermore, as stated in (6), the amplitude $\Phi_{1,L}$ increases with the axial position z and decreases with the tilt angle γ whereas the amplitude $\Phi_{1,R}$ follows the exact opposite trend. As a result, both planes intersect along the dashed line that corresponds to equilibrium positions for this particular winding. Identical conclusions can be drawn regarding the winding A_4 taking into account its reversed dependence to the tilt angle γ.

1) Motor Fluxes: Following an approach identical to that adopted in [8], it can be proved that the electrical and electromagnetic equations related to the drive function only depend on the motor current I_M and on the motor fluxes $\phi_{M,k}$, defined as:

$$\phi_{M,k} = \frac{\phi_{k,L} + \phi_{k,R}}{2} = \Phi_0\cos(p(\delta_k - \alpha)). \tag{7}$$

Regardless of the winding, their amplitude is equal to the flux constant Φ_0 and therefore corresponds to the flux linked by the left and right coils when the rotor is centred, as in a classic permanent magnet machine. Fig. 6(c) illustrates the evolution of the amplitude of the fundamental of the motor

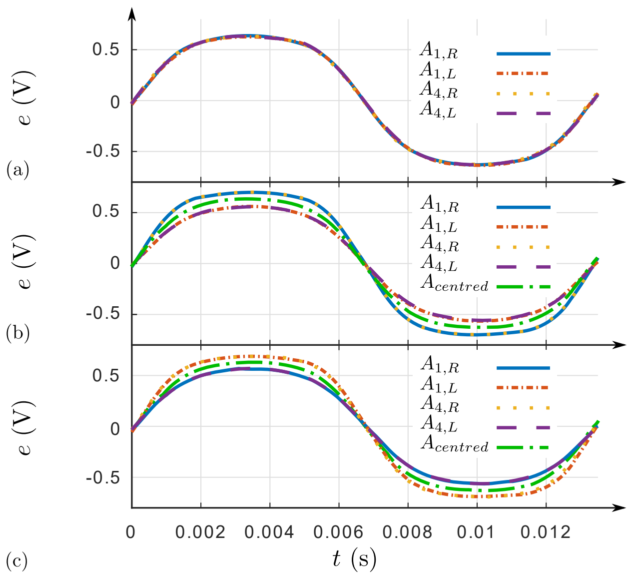

Fig. 5: Time evolution of the electromotive force induced in the left and right coils of the windings A_1 and A_4 for three different relative positions between the rotor and the stator. (a) $z = \lambda = \gamma = 0$. (b) $z = -0.77$ (mm). (c) $\gamma = -1.1$ (deg).

fluxes linked by the windings A_1 and A_4 with the rotor axial position z and the tilt deflection γ. For each winding, the maximal deviation is smaller than 0.5%, therefore endorsing the independence of this flux to the relative position between the rotor and the stator. Lastly, the flux constant Φ_0 is calculated as the mean of both planes, yielding 1.479 (mWb).

2) Suspension Fluxes: Similarly, the electrical and electromagnetic equations linked to the axial and tilt stabilisation are solely dependent on the suspension currents $I_{S,k}$ and on the suspension fluxes $\phi_{S,k}$, expressed as follows:

$$\begin{aligned}\phi_{S,k} &= \phi_{k,L} - \phi_{k,R} = 2zK_z \cos(p(\delta_k - \alpha)) \quad (8)\\ &- 2K_{\beta,p+1}[\gamma \cos((p+1)\delta_k - p\alpha) - \lambda \sin((p+1)\delta_k - p\alpha)]\\ &- 2K_{\beta,p-1}[\gamma \cos((p-1)\delta_k - p\alpha) + \lambda \sin((p-1)\delta_k - p\alpha)].\end{aligned}$$

They correspond to the flux linked by the short-circuited paths formed by the series connection of the left and right coils of each winding and are therefore independent from the flux constant Φ_0. Focusing again on the impact of an axial displacement z and a tilt deflection γ on the windings A_1 ($k = 1$) and A_4 ($k = 10$), the amplitudes of the underlying suspension fluxes reduce to:

$$\begin{aligned}\Phi_{S,A1} &= 2[zK_z - \gamma(K_{\beta,p+1} + K_{\beta,p-1})]\\ \Phi_{S,A4} &= 2[zK_z + \gamma(K_{\beta,p+1} + K_{\beta,p-1})].\end{aligned} \quad (9)$$

Fig. 6(d) depicts the evolution of the amplitude of the fundamental of the suspension fluxes linked by the windings A_1 and A_4 with the rotor axial position z and the tilt deflection γ. As expected, each of these two suspension fluxes cancels in specific relative positions between the rotor and the stator, represented by the dashed lines, that corresponds to the

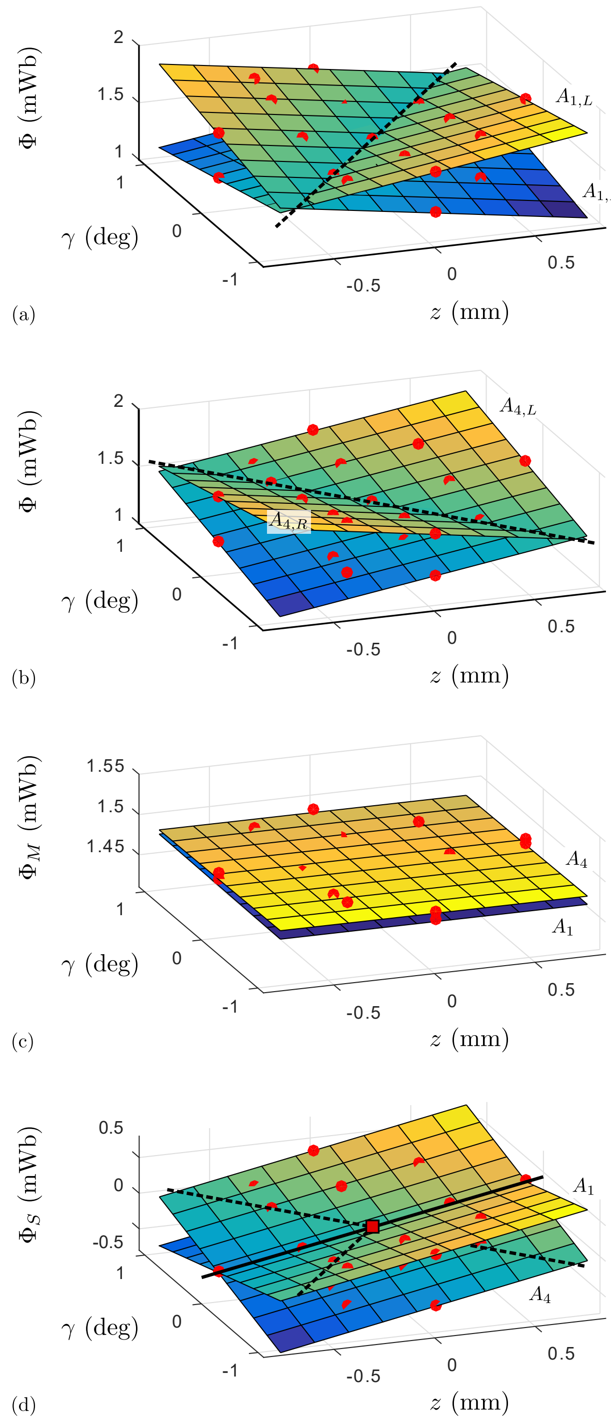

Fig. 6: Evolution of the amplitude of the fundamental of the flux linkages with the axial position z and the tilt deflection γ. (a) Left and right fluxes of the winding A_1. (b) Left and right fluxes of the winding A_4. (c) Motor fluxes of the windings A_1 and A_4. (d) Suspension fluxes of the windings A_1 and A_4.

winding equilibrium points in which no suspension current and therefore no force is produced. Hence, the intersection between these lines, indicated by the square, yields the equilibrium position of this pair of diametrically opposed windings. As

TABLE II: MAGNETIC PARAMETERS OF THE MODEL

	A_1	A_4	$\overline{\{A_1, A_4\}}$	FEM
Φ_0 (mWb)	1.475	1.483	1.479	1.483
K_z (mWb/m)	257.6	261.9	259.7	266.7
$K_{\beta,p+1} + K_{\beta,p-1}$ (mWb/rad)	9.23	9.65	9.44	10.10
$K_{\beta,p-1} - K_{\beta,p+1}$ (mWb/rad)	–	–	–	3.03

stated in (9), the coefficients defining both regression planes are directly proportional to the axial flux gradient K_z as well as to the sum of both tilt flux gradients $K_{\beta,p+1}$ and $K_{\beta,p-1}$. In the same way, assuming that the rotor is axially centred, the analysis of the amplitude of the suspension fluxes linked by the windings A_1 and A_4 with the tilt angle λ allows us to determine the difference between these two flux gradients:

$$\Phi_{S,A1} = \Phi_{S,A4} = 2\lambda |K_{\beta,p-1} - K_{\beta,p+1}|. \tag{10}$$

Their difference being rather small and the method being therefore prone to errors due to a small phase shift between the left and right electromotive forces, no sufficiently reliable value has been extracted from the experimental data. Table II summarises the parameters retrieved from the measurements on each winding as well as those identified through static finite element simulations. In light of the consistency between them, it is decided to separate both tilt flux gradients $K_{\beta,p+1}$ and $K_{\beta,p-1}$ based on the ratio obtained through the numerical simulations, i.e. 0.35/0.65, and the average experimental value of their sum, yielding respectively 3.30 and 6.13 (mWb/rad).

Fig. 7(a) illustrates the time evolution of the electromotive forces induced in the consecutive windings A_6, B_6, C_6 and A_1, whose respective positions are shown in Fig. 4, for a tilt angle γ equal to 0.85 (deg). The thin lines correspond to the experimental data and the thick lines to the Fourier series limited to the third harmonic, underlining that higher order ones are negligible. Remembering that the dynamical model given in (2) neglects the harmonics of the flux linkages, Fig. 7(b) represents the time evolution of the fundamental of the electromotive forces induced in these windings, the solid lines corresponding to the experimental data and the dotted lines to the theoretical expression with the parameters identified above. The deviations in amplitude and phase do not exceed 2.5%, therefore validating both tilt flux gradients $K_{\beta,p+1}$ and $K_{\beta,p-1}$. Let us finally point out the significant phase shift that exists between the suspension voltages induced in the windings A_1 and A_6 resulting from the tilt deflection.

3) Winding configuration: Finally, as mentioned in section II-A, the type of connection between the coils constituting each phase of the armature winding has a significant impact on the bearing behaviour. Fig. 8 illustrates the evolution with the tilt deflection γ of the flux linked by the right coils $A_{1,R}$

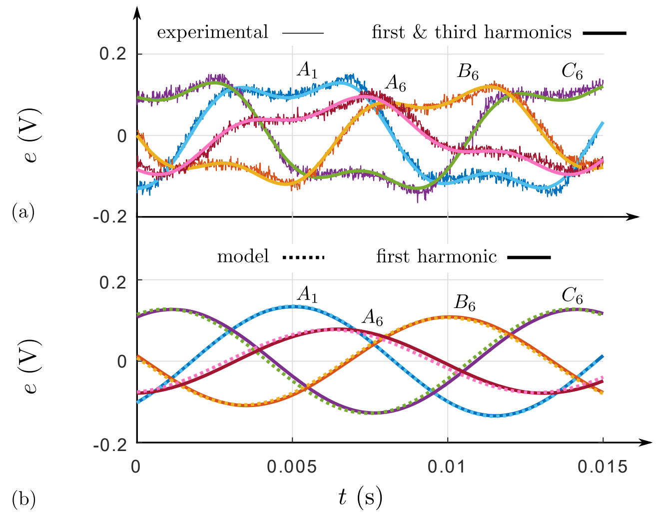

Fig. 7: Time evolution of the electromotive forces induced in the windings A_1, C_6, B_6 and A_6 resulting from a tilt deflection $\gamma = 0.85$ (deg). (a) Experimental data and Fourier series limited to the third harmonic. (b) Fundamental and model.

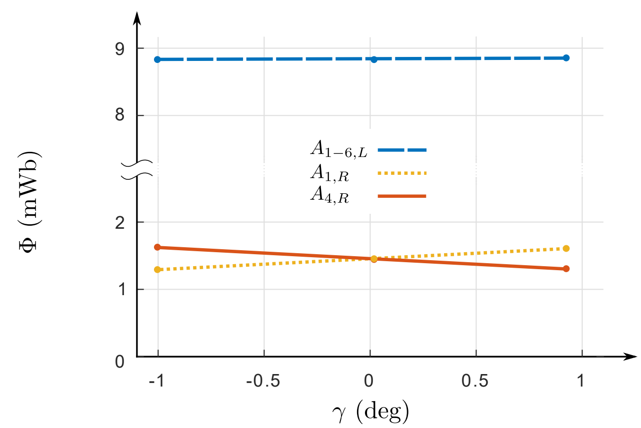

Fig. 8: Evolution with the tilt deflection γ of the fluxes linked by the right coils $A_{1,R}$ and $A_{4,R}$ as well as by the winding formed by the series connection of the p left coils of phase A.

and $A_{4,R}$ as well as by the winding formed through the series connection of the p left coils belonging to phase A. Both former vary by about 10% around the flux linkage related to the equilibrium position whereas the latter does not deviate by more than 0.3%, thus validating its independence from the tilt. Consequently, this specific armature winding connection prevents the appearance of the electrodynamic torque that brings the rotor back to its nominal position but also the torque perpendicular to the tilt that may lead to an instability [11].

C. Bearing Behaviour

As stated in section III, the equations governing the axial and tilt stabilisations are identical to those related to EDTBs alone and are thus independent from the motor currents I_M. In this way, although one single winding achieves both suspension and drive functions, the guidance can be analysed

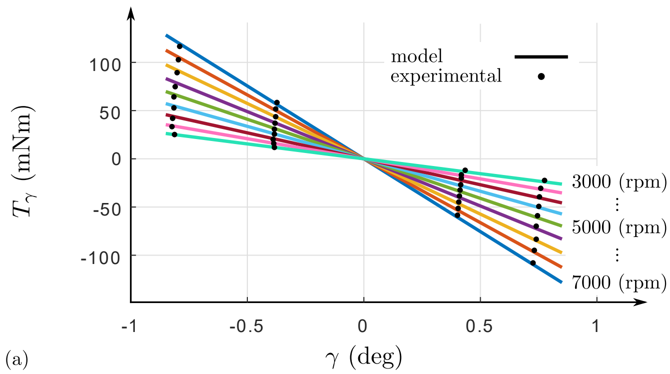

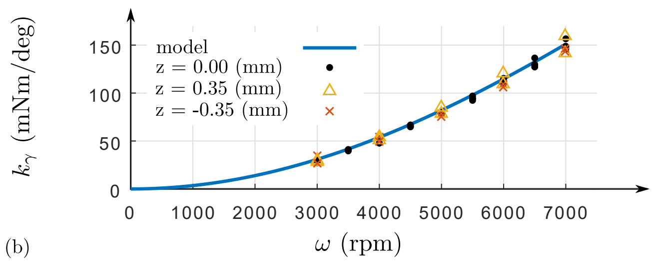

Fig. 9: Tilt stabilisation in quasi-static conditions. (a) Evolution of the torque T_γ with the tilt deflection γ. (b) Evolution of the tilt stiffness k_γ with the spin speed ω.

TABLE III: PARAMETERS OF THE BEARING MODEL

Φ_0 (mWb)	K_z (mWb/m)	$K_{\beta,p+1}$ (mWb/rad)	$K_{\beta,p-1}$ (mWb/rad)
1.479	259.7	3.30	6.13
$L_{c,p}$ (μH)	$L_{c,p+1}$ (μH)	$L_{c,p-1}$ (μH)	R (mΩ)
21.26	16.80	25.75	141

separately from the actuation. To this end, the supply voltage is removed from the armature winding, the left and right coils being therefore connected in series, while the rotor is driven through an external DC motor.

Fig. 9(a) illustrates the evolution of the restoring torque T_γ with the tilt angle γ when the rotor is in its axial equilibrium position, i.e. $z = 0$, the dots corresponding to the experimental data for several spin speeds ω and the straight lines to the theoretical expression given in (3) with the parameters identified above, summarised in Table III. The discrepancies between them, that may result from the third harmonic, do not exceed 8.5%, thus allowing us to validate, in quasi-static conditions, the electromechanical model (2) describing the tilt behaviour. Fig. 9(b) represents the evolution of the tilt stiffness k_γ with the rotor spin speed ω, the straight line corresponding to the model, the dots to the experimental data obtained in the axial nominal position and the triangles as well as the crosses when the rotor is axially decentred. The stiffness being positive, the electrodynamic phenomena tend to bring the system in its nominal position. Furthermore, for the speed range considered here, the stiffness increases up to reach 31 (mNm/deg) at 3000 (rpm) and 150 (mNm/deg) at 7000 (rpm). Finally, the deviations between the theoretical curve and the decentred measurements remain below 13%, underlining the limited impact of the rotor axial position z on the tilt stiffness.

VI. CONCLUSION

This paper presents the theoretical and experimental characterisation of the tilt stabilisation that can be achieved within electrodynamic thrust self-bearing machines. The prototype and its dedicated test rig allowing us to investigate the spin, axial and tilt behaviours are described. In-depth analyses of the variations of the winding flux linkage with the axial and tilt deflections, lying at the basis of the electrodynamic phenomena, are performed, notably corroborating the corresponding theoretical expression as well as the linearisation ensuing from the assumption of small displacements. The impact of the type of connection between the coils constituting the armature winding is also studied, underlining in particular that connecting the p coils of each phase in series on both sides prevents the appearance of torques in reaction to the rotor tilt. Finally, the operation principle as well as the electromechanical model related to the tilt levitation are validated in quasi-static conditions, highlighting the generation of a restoring tilt stiffness reaching up to 150 (mNm/deg) at 7000 (rpm) as well as the limited influence of the rotor axial position on the latter.

REFERENCES

[1] R. Oishi, S. Horima, H. Sugimoto, and A. Chiba, “A novel parallel motor winding structure for bearingless motors,” *IEEE Transactions on Magnetics*, vol. 49, no. 5, pp. 2287–2290, May 2013.

[2] H. Mitterhofer, B. Mrak, and W. Gruber, “Comparison of high-speed bearingless drive topologies with combined windings,” *IEEE Transactions on Industry Applications*, vol. 51, no. 3, pp. 2116–2122, May 2015.

[3] W. K. S. Khoo, K. Kalita, and S. D. Garvey, “Practical implementation of the bridge configured winding for producing controllable transverse forces in electrical machines,” *IEEE Transactions on Magnetics*, vol. 47, no. 6, pp. 1712–1718, June 2011.

[4] V. Kluyskens, C. Dumont, and B. Dehez, “Description of an electrodynamic self-bearing permanent magnet machine,” *IEEE Transactions on Magnetics*, vol. 53, no. 1, pp. 1–9, Jan 2017.

[5] V. Kluyskens, J. Van Verdeghem, C. Dumont, and B. Dehez, “Experimental investigations on a heteropolar electrodynamic bearing-self-bearing motor,” *Proc. 16th International Symposium on Magnetic Bearings (ISMB)*, August 2018.

[6] J. Van Verdeghem, C. Dumont, V. Kluyskens, and B. Dehez, “Linear state-space representation of the axial dynamics of electrodynamic thrust bearings,” *IEEE Transactions on Magnetics*, vol. 52, no. 10, pp. 1–12, Oct 2016.

[7] H. K. Asper and S. Siposs, *Passive Magnetic bearing with integrated motor generator for flywheel applications*. Dresden, Germanny: 8th International Symposium On Magnetic Suspension Technology, 2005.

[8] J. Van Verdeghem, M. Lefebvre, V. Kluyskens, and B. Dehez, “Dynamical modelling of passively levitated electrodynamic thrust self-bearing machines,” *IEEE Transactions on Industry Applications*, vol. 55, no. 2, pp. 1–1, 2018.

[9] J. Van Verdeghem, V. Kluyskens, and B. Dehez, “Experimental validation and characterisation of a passively levitated electrodynamic thrust self-bearing motor,” *Proc. 21th International Conference on Electrical Machines and Systems (ICEMS)*, October 2018.

[10] K. D. Bachovchin, J. F. Hoburg, and R. F. Post, “Stable levitation of a passive magnetic bearing,” *IEEE Transactions on Magnetics*, vol. 49, no. 1, pp. 609–617, Jan 2013.

[11] J. Van Verdeghem, V. Kluyskens, and B. Dehez, “Five degrees of freedom linear state-space representation of electrodynamic thrust bearings,” *Journal of Sound and Vibration*, vol. 405, pp. 48 – 67, 2017.